The Journal of Chemical Physics

Coarse-grained simulation of the translational and rotational diffusion of globular proteins by dissipative particle dynamics

Cite as: J. Chem. Phys. **153**, 234902 (2020); https://doi.org/10.1063/5.0025620
Submitted: 17 August 2020 . Accepted: 30 November 2020 . Published Online: 15 December 2020

Jiachen Wei, Yawei Liu, and Fan Song

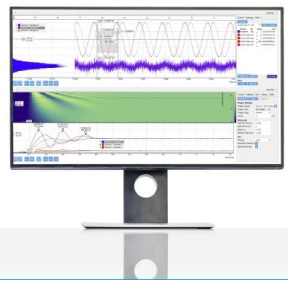

AIP Publishing

The Journal of Chemical Physics ARTICLE scitation.org/journal/jcp

Coarse-grained simulation of the translational and rotational diffusion of globular proteins by dissipative particle dynamics

Cite as: J. Chem. Phys. 153, 234902 (2020); doi: 10.1063/5.0025620
Submitted: 17 August 2020 • Accepted: 30 November 2020 •
Published Online: 15 December 2020

Jiachen Wei,[1,2,a)] Yawei Liu,[3,a)] and Fan Song[1,2]

AFFILIATIONS

[1]State Key Laboratory of Nonlinear Mechanics, Institute of Mechanics, Chinese Academy of Sciences, Beijing 100190, China
[2]School of Engineering Science, University of Chinese Academy of Sciences, Beijing 100049, China
[3]ARC Centre of Excellence in Exciton Science, School of Chemistry, University of Sydney, Sydney, New South Wales 2006, Australia

[a)]**Authors to whom correspondence should be addressed:** weijiachen@lnm.imech.ac.cn and yawei.liu@sydney.edu.au

ABSTRACT

With simplified interactions and degrees of freedom, coarse-grained (CG) simulations have been successfully applied to study the translational and rotational diffusion of proteins in solution. However, in order to reach larger lengths and longer timescales, many CG simulations employ an oversimplified model for proteins or an implicit-solvent model in which the hydrodynamic interactions are ignored, and thus, the real kinetics are more or less unfaithful. In this work, we develop a CG model based on the dissipative particle dynamics (DPD) that can be universally applied to different types of proteins. The proteins are modeled as a group of rigid DPD beads without conformational changes. The fluids (including solvent and ions) are also modeled as DPD beads. The electrostatic interactions between charged species are explicitly considered by including charge distributions on DPD particles. Moreover, a surface friction between the protein and fluid beads is applied to control the slip boundary condition. With this model, we investigate the self-diffusion of a single globular protein in bulk solution. The translational and rotational diffusion coefficients of the protein can be tuned by the surface frictional constant to fit the predictions of the Stokes–Einstein (SE) relation. We find that both translational and rotational diffusion coefficients that meet with the prediction of the SE relation based on experimental results of the hydrodynamic radius are reached at almost the same frictional constant for different types of proteins. Such scaling behavior indicates that the model can be applied to simulate the translational and rotational diffusion together for various types of proteins.

I. INTRODUCTION

The diffusion of proteins in solution is a type of thermal motion that governs various phenomena such as adsorption at the interface,[1–6] molecular recognition,[7–9] phoretic motion,[10–12] and transport in nano-confined systems.[13–22] When there is no chemical potential gradient, the process reduces to the self-diffusion of the protein, including the random redistribution (i.e., translational diffusion) and the random reorientation (i.e., rotational diffusion) in space. Accurate determination of the translational[16,22–24] and rotational[21,25–31] dynamics provides the basis for the characterization of individual proteins and their complexes and for the understanding of the transport of proteins in a non-equilibrium system.

Experimentally, the translational and rotational dynamics of proteins can be determined by fluorescence spectroscopy,[32–34] nanopore sensing,[7–9] nuclear magnetic resonance (NMR) relaxation,[27,35,36] etc. However, the experimental results of the diffusion coefficients for certain types of protein usually vary across literature studies, due in part to the difference in measuring conditions (e.g., temperature, protein concentration, viscosity of the solvent, and pH). For better understanding of the large variance of the

experimental data and for the prediction of transport in more complex media, we also entail numerical tools to determine the diffusion coefficients of proteins. The simulated results are sensitive to the choice of the model for the protein solution and the corresponding force field. For instance, based on the colloidal model, the protein is deemed a single bead that ignores all internal structures.[37] Such an approach is efficient in simulating the collective diffusion in macromolecular crowding but too coarse-grained to characterize the self-diffusion of a single protein in solution. All-atom molecular dynamics[27–29] is more suited for the determination of the local dynamics (including the redistribution and reorientation of all sub-domains), but it is computationally expensive and normally limited in the regime of a small simulation box. A more appropriate approach is to simulate the protein solution with a well-designed model at a certain degree of coarse-graining.[37,38]

There have been reported some well-established methods for simulating proteins in solution with coarse-grained molecular dynamics[38–41] (CGMD). Yet, it is somehow difficult in CGMD simulations to properly address hydrodynamic interactions as it ignores the degrees of freedom that are responsible for dissipation. The hydrodynamic interactions between coarse-grained particles are introduced in forms of pairwise-additive approximation for Brownian dynamics[14,17,18] (BD). This technique can be applied to determining the equilibrium states but is not ideally suitable for problems emphasizing specific transient behaviors or detailed hydrodynamic interactions.

By contrast, dissipative particle dynamics (DPD) is developed for simulating the hydrodynamic behavior of fluids and soft matter by explicitly accounting for the drag and random forces between soft coarse-grained beads.[42–45] DPD provides an accurate bridge from the atomic to the hydrodynamic scale by enabling various levels of graining with simple algorithms, which serves as a practical choice for the determination of the thermodynamic and kinetic properties of proteins in solution.[34,46–50] For instance, models with the backbone and side-chains are invented for DPD simulations[46–48] based on the bottom-up approach to mimic the conformational transformations of proteins. Simulations of the aggregation and self-assembly of proteins at higher concentrations are carried out with more coarse-grained models, with inter-particle potentials tuned by experimental results.[34,49] To our knowledge, however, there is a lack of DPD simulations on the self-diffusion or transport of globular proteins. We still need a versatile coarse-grained method for simulations with accurate electrostatics between charged species, and proper slip-boundary conditions between the protein and the fluid.

We, therefore, in this work introduce a DPD model with explicit electrostatic interactions[51,52] and tunable surface frictions[53] to simulate the diffusion of globular proteins. The results show that the method is effective to characterize both the translational and rotational diffusion coefficients with the same DPD parameters for different types of proteins. In the remainder of this paper, we first introduce the model and the simulation methods and then proceed to analyze the results of the simulations. Taking lysozyme as an example, we are, in particular, interested in the dependence of its diffusion coefficients on the system size and the slip-boundary condition. Comparisons with other globular proteins are then presented.

II. SIMULATION METHOD

A. Model

We perform DPD simulations of the protein solution in a cubic box. As shown in Fig. 1(a), the fluids, including water (w), cation (c), and anion (a), are modeled as DPD beads. We set the coarse-graining degree $\xi = 4$, with one fluid bead representing either four water molecules (for a w bead) or three water molecules plus one cation/anion (for a c or a bead). The mass of the water bead m_w, the cutoff radius of the water bead r_w, the temperature of the system T, the corresponding energy k_BT (with k_B being the Boltzmann constant), and the unit charge q_e are chosen as the reduced units, which correspond to $m_w = 1.2 \times 10^{-25}$ kg, $r_w = 0.71$ nm, $T = 298$ K, $k_BT = 4.1 \times 10^{-21}$ J, and $q_e = 1.6 \times 10^{-19}$ C in real units. The full list of reduced and real units is presented in Table I. Unless specified, reduced units will be used in the remainder of this paper. The protein is modeled as a group of rigid DPD beads (p) neglecting conformational changes, with each bead representing one amino acid (see the supplementary material for more details). The beads can be either the mono-sized model (MSM) or the poly-sized model (PSM), as shown in Fig. 1(b). For the MSM, all protein beads are of the same cutoff radius $r_c = 1.0$ and mass $m = M/N_p$, where M and N_p, respectively, denote the total mass and the number of amino acids of the protein. For the PSM, the radius and mass of the beads depend on the type of amino acid (see the supplementary material for more details). The charge of the bead equals the sum of all atomic charges of the corresponding amino acid, and the net charge of the protein equals the sum of all charges of beads. See Table II for the full list of properties for different types of beads.

All fluid beads (i.e., w, c, and a) interact with each other via DPD interactions including a conservative force $\boldsymbol{F}_{ij}^C$, a dissipative force $\boldsymbol{F}_{ij}^D$, and a random force $\boldsymbol{F}_{ij}^R$ given by

$$\begin{aligned} \boldsymbol{F}_{ij}^C &= A_{ij}(1 - r_{ij}/r_c)\boldsymbol{e}_{ij}, \text{ for } r_{ij} < r_c; \\ \boldsymbol{F}_{ij}^D &= -\gamma_{ij}(1 - r_{ij}/r_c)^2(\boldsymbol{e}_{ij} \cdot \boldsymbol{v}_{ij})\boldsymbol{e}_{ij}, \text{ for } r_{ij} < r_c; \\ \boldsymbol{F}_{ij}^R &= \sqrt{2k_B\mathrm{T}\gamma_{ij}}(1 - r_{ij}/r_c)\theta_{ij}(\delta t)^{-1/2}\boldsymbol{e}_{ij}, \text{ for } r_{ij} < r_c, \end{aligned} \tag{1}$$

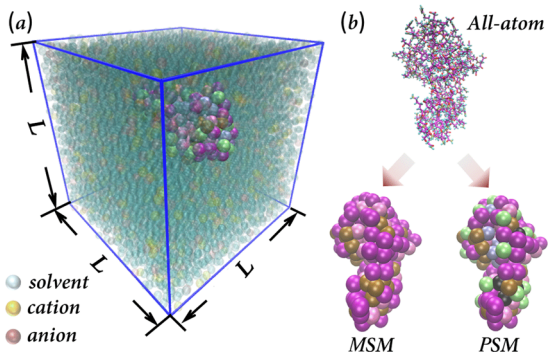

FIG. 1. (a) Simulation box of the globular protein submerged in the fluid consisting of solvent (cyan), cation (yellow), and anion (red) beads. (b) All-atomic protein is represented by either the mono-sized model (MSM) or the poly-sized model (PSM).

TABLE I. Comparisons of quantities measured in reduced and real units.

Quantities	In reduced unit	In real unit
r_w	1.0	0.71 nm
m_w	1.0	1.2×10^{-25} kg
T	1.0	298 K
k_BT	1.0	4.1×10^{-21} J
q_e	1.0	1.6×10^{-19} C
ρ	3.0	997 kg/m^3
δt	0.002	8 fs
Γ	12.65	3.7×10^{-29} J · m
η	20.34	0.89 mPa · s
μ	6.78	8.9×10^{-7} m^2/s

where r_{ij} is the center-to-center distance between beads i and j, $\boldsymbol{e}_{ij} = \boldsymbol{r}_{ij}/r_{ij}$ is the unit vector, A_{ij} is the maximum repulsion, γ_{ij} is the dissipative constant, $\boldsymbol{v}_{ij}$ is the vector difference in velocities between the two beads, θ_{ij} is a Gaussian white noise variable with $\theta_{ij} = \theta_{ji}$, and δt is the simulation time step. All these three forces vanish when $r_{ij} \geq r_c$. To match the compressibility and viscosity of water, we set $A_{ij} = 104$ and $\gamma_{ij} = 630$ between fluid beads (see the supplementary material).

Note that Eq. (1) cannot be applied to interactions between fluid and protein beads, since it overestimates both the translational and rotational diffusion coefficients of the protein without well-controlled slip velocity at the interface (see the supplementary material for more details). To solve this, we employ forces for tunable-slip DPD (TDPD) to describe interactions between protein beads (p) and fluid beads, including a conservative force $\boldsymbol{F}_{ij}^C$, a frictional force $\boldsymbol{F}_{ij}^F$, and a random force $\boldsymbol{F}_{ij}^R$ with the latter two depending on the relative velocity between protein and fluid beads, which are given by

$$\begin{aligned} \boldsymbol{F}_{ij}^C &= A_{ij}(1 - r_{ij}/r_c)\boldsymbol{e}_{ij}, \text{ for } r_{ij} < r_c; \\ \boldsymbol{F}_{ij}^F &= -\nu_{ij}(1 - r_{ij}/r_c)\boldsymbol{v}_{ij}, \text{ for } r_{ij} < r_c; \\ \boldsymbol{F}_{ij}^R &= \sqrt{2k_B\mathrm{T}\nu_{ij}(1 - r_{ij}/r_c)}\theta_{ij}(\delta t)^{-1/2}\boldsymbol{v}_{ij}/v_{ij}, \text{ for } r_{ij} < r_c, \end{aligned} \tag{2}$$

with ν_{ij} being the frictional constant. In this work, ν_{ij} is varied to test the effect of the frictional force on the diffusion coefficient. Parameters for the conservative force (i.e., A_{ij} and r_c) between the protein and the fluid are derived and scaled from the less coarse-grained DPD model.[48] See Table III for the full list of interaction parameters used in this paper (unless otherwise specified) and the supplementary material for more discussions.

The electrostatic interaction between charged beads (i.e., p, c, and a) is described by the smeared-charge Coulombic potential (SCC), which is written as

$$U_{ij}^{col}(r_{ij}) = \frac{\Gamma z_i z_j}{4\pi r_{ij}}\left[1 - (1 + r_{ij}/\lambda)e^{-2r_{ij}/\lambda}\right], \tag{3}$$

where $\Gamma = q_e^2/(\varepsilon_0\varepsilon_w) = 12.65$ is the permittivity coupling parameter (with ε_0 being the dielectric constant for the vacuum and $\varepsilon_w = 78.3$ being the relative permittivity of water). z_i and z_j are the valence of beads i and j, respectively. λ denotes the effective smearing length that is determined by the charge density distribution as $\rho(r) = \left(q/\pi\lambda^3\right)\exp(-2r/\lambda)$, where the charge of the bead $q = zq_e$. A cutoff $r_c^{col} = 3.5$ is used for U_{ij}^{col}, while long-range Coulombic interactions including contribution from periodic images are computed with the particle–particle particle–mesh (PPPM) method. For the ionic beads, we have $q = 1.0$ for cations and $q = -1.0$ for anions.

B. Simulation details

We simulate the submerged protein in an $L \times L \times L$ cubic box with periodic boundary conditions implemented in all three dimensions. A total number of N_f fluid beads (w, c, and a) are maintained at the fixed density $\rho = 3.0$ (or 997 kg/m^3 in real units) and temperature $T = 1.0$ in the NVT ensemble. Counter-ions are added to ensure the whole system is neutral. All simulations are carried out by using the parallel software package LAMMPS.[54] The velocity-Verlet algorithm with a time step of $\delta t = 0.002$ is used to integrate the equations of motion.

All initial configurations are prepared as follows. First, all water beads are uniformly distributed on a FCC crystal lattice, and the protein (consisting of N_p beads) is placed at the center of the simulation

TABLE II. Comparisons of different types of DPD beads.

Bead type		Mass	Charge	Corresponding molecules or amino acids
w		1.0	0.0	Four water molecules
c		1.0	1.0	Three water molecules + one cation
a		1.0	−1.0	Three water molecules + one anion
MSM	p_h	M/N_p	−1.0–1.0	ASP GLU ASN PRO GLN SER THR LYS ARG
	p_m	M/N_p	0.0	ALA GLY CYS HIS TYR
	p_t	M/N_p	0.0	ILE LEU VAL PHE MET TRP
PSM	p_{hs}	m_{hs}	−1.0–1.0	ASP ASN PRO SER THR
	p_{hl}	m_{hl}	−1.0–1.0	LYS ARG GLU GLN
	p_{ms}	m_{ms}	0.0	ALA GLY CYS
	p_{ml}	m_{ml}	0.0	HIS TYR
	p_{ts}	m_{ts}	0.0	ILE LEU VAL
	p_{tl}	m_{tl}	0.0	PHE MET TRP

TABLE III. Parameters for DPD, TDPD, and SCC interactions between different types of beads (unless otherwise specified).

DPD for fluids	A_{ij}	γ_{ij}	r_c
$w/c/a - w/c/a$	104	630	1.0
TDPD for the MSM	A_{ij}	ν_{ij}	r_c
$w/c/a - p_h$	104	0–200	1.0
$w/c/a - p_m$	111	0–200	1.0
$w/c/a - p_t$	127	0–200	1.0
TDPD for the PSM	A_{ij}	ν_{ij}	r_c
$w/c/a - p_{hs}$	$104(r_w/r_c^{hs})$	0–200	r_c^{hs}
$w/c/a - p_{hl}$	$104(r_w/r_c^{hl})$	0–200	r_c^{hl}
$w/c/a - p_{ms}$	$111(r_w/r_c^{ms})$	0–200	r_c^{ms}
$w/c/a - p_{ml}$	$111(r_w/r_c^{ml})$	0–200	r_c^{ml}
$w/c/a - p_{ts}$	$127(r_w/r_c^{ts})$	0–200	r_c^{ts}
$w/c/a - p_{tl}$	$127(r_w/r_c^{tl})$	0–200	r_c^{tl}
SCC	Γ	λ	r_c^{col}
$c/a/p - c/a/p$	12.65	0.25	3.5

TABLE IV. Comparison of simulation sizes for DPD and all-atom simulations. R_h and L, respectively, denote the experimental hydrodynamic radius of the protein and the side length of the simulation box (in units of r_w). N_p and N_f, respectively, denote the number of DPD beads for the protein and fluid. N_p^{aa} and N_f^{aa} are the corresponding number of atoms in all-atom simulations. The values of N_f and N_f^{aa} are for systems with lysozyme.

Protein beads (p)				
Protein type	PDB code	R_h [r_w]	N_p	N_p^{aa}
Ubiquitin	1ubq	2.10–2.21[16,22,55]	76	602
Lysozyme	253l	2.63–2.89[56–58]	164	1306
β-Lactoglobulin	1beb	3.80–4.22[59,60]	312	2981
Streptavidin	4jo6	3.97–4.54[7,16]	531	3984
Fluid beads ($w/c/a$)				
L [r_w]	N_f	N_f^{aa}		
16	12 131	145 554		
20	23 843	286 098		
24	41 315	495 762		
32	98 147	1 177 746		
40	191 843	2 302 098		

box. To keep $\rho = 3.0$ constant in bulk, water beads are randomly added or deleted in the next 4×10^6 simulation steps. $|Q_p/q_e|$ water beads are randomly chosen and replaced by cation or anion beads to neutralize the system, where Q_p is the net charge of the protein. Subsequently, a long run (at least 2×10^7 steps) is performed to obtain the diffusion coefficients, which are determined by averaging at least five independent runs. The trajectories are collected over 4×10^3 configurations separated by 5×10^3 simulation steps. We note that this coarse-grained system has a particle number at least one order of magnitude smaller than that of the all-atomic model, see Table IV.

The translational diffusion coefficient D_t of the protein is measured from the mean squared displacement (MSD) of the center of mass (COM), which is written as

$$D_t = \lim_{t\to\infty} \frac{1}{6t} \left\langle (\boldsymbol{r}(t) - \boldsymbol{r}(0))^2 \right\rangle, \tag{4}$$

where $\boldsymbol{r}(t)$ denotes the COM position of the protein at time t. Since the long-wavelength hydrodynamic modes are affected by the periodic images, the magnitude of D_t measured from Eq. (4) should increase with the box size. By summing over all periodic images of the Oseen tensor,[16,24] theoretically, the translational diffusion coefficient in bulk D_t^∞ (with the non-slip boundary condition) is predicted as

$$D_t^\infty = D_t(L) + \frac{2.837 k_B T}{6\pi\eta L}, \tag{5}$$

where η represents the shear viscosity of the solvent.

The rotational diffusion coefficients D_{ri} of the protein can be derived from the angular mean squared displacement[61,62] (AMSD), which is expressed as

$$D_{ri} = \lim_{t\to\infty} \frac{1}{2t} \left\langle (\varphi_i(t) - \varphi_i(0))^2 \right\rangle, \tag{6}$$

where $\varphi_i(t)$ denotes the angular position about the axis i at time t, with $i \in [x, y, z]$ corresponding to principal axes of inertia in the decreasing order of eigenvalues of the inertia tensor. The mean rotational diffusion coefficient D_r can then be estimated as[61,62]

$$D_r = (D_{\mathrm{rx}} + D_{\mathrm{ry}} + D_{\mathrm{rz}})/3. \tag{7}$$

By assuming $D_{rx} < D_{ry} < D_{rz}$, the anisotropy Λ and rhombicity Ω of the rotational diffusion tensors[27] are, respectively, defined as

$$\Lambda = \frac{2D_{\mathrm{rz}}}{D_{\mathrm{rx}} + D_{\mathrm{ry}}} \quad \text{and} \quad \Omega = \frac{1.5(D_{\mathrm{ry}} - D_{\mathrm{rx}})}{D_{\mathrm{rz}} - 0.5(D_{\mathrm{rx}} + D_{\mathrm{ry}})}. \tag{8}$$

Both Λ and Ω measure the degree of directional asymmetry of the diffusion tensor. While Λ measures the difference between the largest diffusion tensor and the other two, Ω gives information on the difference between the smallest and second-smallest diffusion tensors. The periodic boundary conditions may also affect the rotational diffusion. Linke *et al.*[25,26] expect the rotational diffusion coefficient in bulk D_r^∞ depends on the box size as

$$D_r^\infty = D_r(L) + \frac{k_B T}{6\eta L^3}. \tag{9}$$

D_r can also be determined from the re-orientational time correlations,[21,63] angular momentum autocorrelations,[29] Einstein–Smoluchowski relation,[61] or time-dependent covariance of the quaternions.[25,27] The values of D_r are compared with that determined from re-orientational time correlations in the supplementary material to check if the motion can be described as small-step diffusion in our simulations.[62,63]

We note that the diffusion coefficients can also be predicted from the hydrodynamic radius of the protein based on the Stokes–Einstein (SE) relation,

$$D_t^{SE} = \frac{k_B T}{6\pi\eta R_h} \text{ and } D_r^{SE} = \frac{k_B T}{8\pi\eta R_h^3}, \tag{10}$$

where D_t^{SE} and D_r^{SE}, respectively, denote the translational and rotational diffusion coefficients predicted by the SE relation. R_h denotes the hydrodynamic radius of the protein (i.e., the mean value of experimental results shown in Table IV). We then define the dimensionless translational diffusion coefficient in bulk $\widetilde{D}_t^{\infty}$ and the dimensionless rotational diffusion coefficient in bulk $\widetilde{D}_r^{\infty}$ as

$$\widetilde{D}_t^{\infty} = \frac{D_t^{\infty}}{D_t^{SE}} = \frac{6\pi\eta R_h D_t^{\infty}}{k_B T} \text{ and } \widetilde{D}_r^{\infty} = \frac{D_r^{\infty}}{D_r^{SE}} = \frac{8\pi\eta R_h^3 D_r^{\infty}}{k_B T}. \tag{11}$$

The translational and rotational diffusion coefficients predicted by the SE relation are obtained at $\widetilde{D}_t^{\infty} = 1$ and $\widetilde{D}_r^{\infty} = 1$, respectively.

The Green function $G_i(\theta_i, t)$, with θ_i being the angular position of the axis i, is used to probe the time evolution for the orientations accessed by the protein during the simulation,[64,65] which can be calculated as

$$G_i(\theta_i, t) = \left\langle \delta\left\{\cos^{-1}[\boldsymbol{u}_i(0)\cdot\boldsymbol{u}_i(t)] - \theta_i\right\}\right\rangle, \tag{12}$$

where δ denotes the delta function and $\boldsymbol{u}_i$ is a unit vector along the inertial axis i.

III. RESULTS AND DISCUSSION

A. Effects of box size

Figure 2 presents the dependence of the dimensionless translational diffusion coefficient $\widetilde{D}_t = D_t/D_t^{SE}$ and dimensionless rotational diffusion coefficient $\widetilde{D}_r = D_r/D_r^{SE}$ of lysozyme in the finite system on R_h/L (with $R_h = 2.76$ being the hydrodynamic radius of lysozyme and L being the side length of the simulation box). For both the MSM and the PSM, as shown in Fig. 2(a), we observe the linear decrease in $\widetilde{D}_t$ with the inverse of the box length. The slope of the fitting lines s_t varies from −2.89 to −2.68 at different values of the fluid–protein frictional constant ν, in accord with the theoretical prediction of Eq. (5) (i.e., $s_t = -2.837$). The dimensionless translational diffusion coefficient in bulk $\widetilde{D}_t^{\infty}$ can then be derived from the intercept of the fitting curve.

Similar to previous determinations of D_r by re-orientational time correlations,[21] we do not obtain the obvious size effect on the rotational diffusion coefficient for both the MSM and the PSM, as shown in Fig. 2(b). This is because D_r scales with $1/L^3$ rather than $1/L$ according to Eq. (9). The decay of D_r due to hydrodynamics with periodic images is thus negligibly small even in the smallest box used in this work (i.e., $L = 16$). We estimate the dimensionless rotational diffusion coefficient in bulk $\widetilde{D}_r^{\infty}$ as the average value of $\widetilde{D}_r$ calculated at different box sizes.

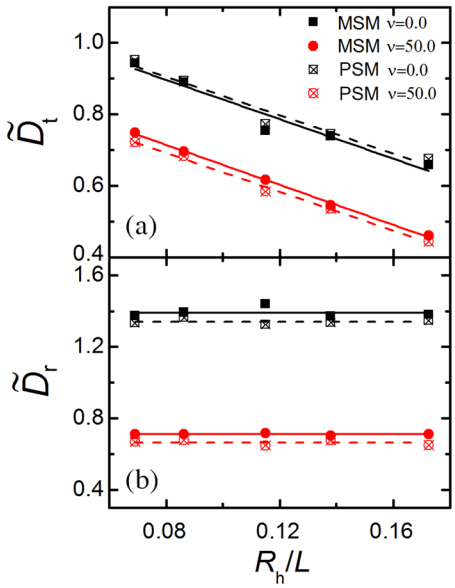

FIG. 2. Size effects on the (a) dimensionless translational diffusion coefficient $\widetilde{D}_t$ and (b) dimensionless rotational diffusion coefficient $\widetilde{D}_r$ of lysozyme in the finite system. The solid (for the MSM) and dashed (for the PSM) lines are linear fittings.

We do not observe the size effect on the Green function $G(\theta_i, t)$, anisotropy Λ, or rhombicity Ω of the rotational diffusion tensors, see the supplementary material for more details.

B. Effects of boundary condition

The effect of the slip boundary condition on the diffusion coefficient in bulk is presented in Fig. 3. It is found that both $\widetilde{D}_t^{\infty}$ and $\widetilde{D}_r^{\infty}$ decay exponentially with the fluid–protein frictional constant ν, which can be written as $\widetilde{D}_t^{\infty} = A_t e^{-\lambda_t \nu} + \widetilde{D}_t^0$ and $\widetilde{D}_r^{\infty} = A_r e^{-\lambda_r \nu} + \widetilde{D}_r^0$, respectively. At fixed ν, $\widetilde{D}_t^{\infty}$ and $\widetilde{D}_r^{\infty}$ determined from the PSM (black) are always slightly smaller than those determined from the MSM (red). This indicates that the geometric and chemical heterogeneity could slightly suppress the diffusion of the protein. For both models, the same decay constants $\lambda_t \sim 0.021$ and $\lambda_r \sim 0.016$ are obtained for the translational and rotational diffusion coefficients, respectively. In Fig. 3(a), the diffusion coefficient that follows the prediction of the SE relation (i.e., $\widetilde{D}_t^{\infty} = 1$ as indicated by the dashed line) is obtained at $\nu_t = 20$ for the MSM and $\nu_t = 16$ for the PSM, while $\widetilde{D}_r^{\infty} = 1$ in Fig. 3(b) is obtained at $\nu_r = 12$ for both the MSM and the PSM. For simultaneous characterizations of both translational and rotational diffusion, we expect the discrepancy $\Delta\nu = |\nu_r - \nu_t|$ to be as small as possible. The results indicate that the MSM is fine enough to characterize the diffusion of the protein with slightly larger $\Delta\nu = 8$ compared to $\Delta\nu = 4$ for the PSM.

Figure 4 compares the effect of ν on the anisotropy Λ and rhombicity Ω of the rotational diffusion tensors for the MSM and PSM.

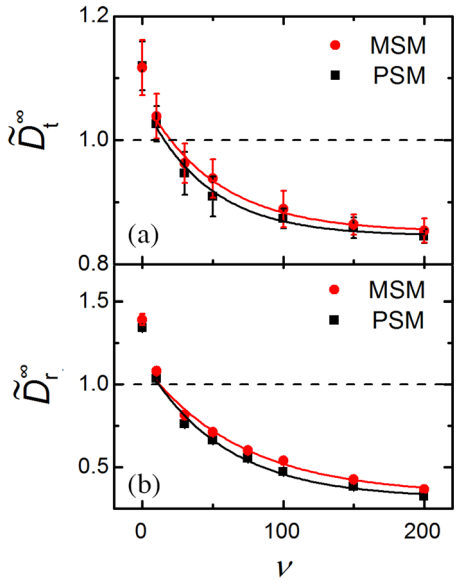

FIG. 3. Dependence of the (a) dimensionless translational diffusion coefficient in bulk $\widetilde{D}_t^{\infty}$ and (b) dimensionless rotational diffusion coefficient in bulk $\widetilde{D}_r^{\infty}$ on the fluid–protein frictional constant ν, for both the MSM (red) and the PSM (black). The solid lines are fitting curves with exponential decay (note that results at $\nu = 0$ are not used). The dashed lines are for $\widetilde{D}_t^{\infty} = 1$ and $\widetilde{D}_r^{\infty} = 1$.

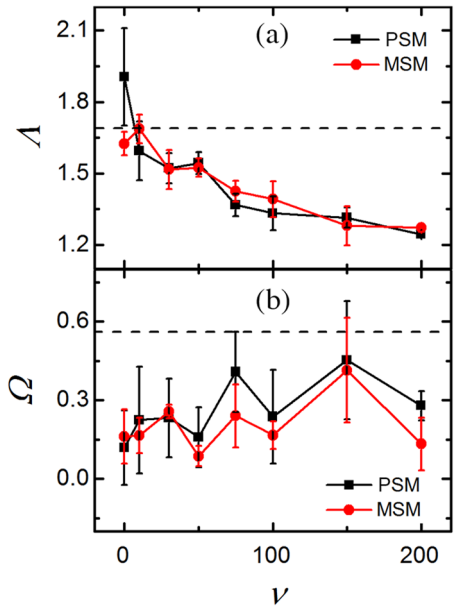

FIG. 4. Dependence of (a) anisotropy Λ and (b) rhombicity Ω of the rotational diffusion tensors on the frictional constant ν. The dashed lines are results derived from all-atom MD simulations.[66]

Figure 4(a) shows that the magnitude of Λ is negatively related to ν for both the MSM and the PSM. The all-atom simulation result indicated by the dashed line ($\Lambda_{aa} = 1.69$) is reached at around $\nu \sim 10$, at which D_r^{∞} comparable to the experimental result is also obtained. As shown in Fig. 4(b), Ω depends less sensitively on ν, and our DPD results seem to underestimate the magnitude of Ω compared with the all-atom simulation result (dashed line). A slightly larger average value of Ω is obtained by the PSM than the MSM for $\nu \geq 50$. The difference between the PSM and the MSM is, however, negligibly small within measurement error. This again indicates size heterogeneity of the protein beads has a very limited effect on the diffusion tensors.

The slow-down of rotational diffusion upon fluid–protein frictional forces can also be demonstrated by the Green function $G_i(\theta, t)$ shown in Fig. 5. For $\nu < 100$, the shape of $G_z(\theta, t* = 5$ ns) corresponding to the third principal axis of inertia z at $t* = 5$ ns for the PSM changes sharply with ν. This indicates the reorientation of the protein is effectively suppressed with the increase in the frictional forces. The shape of G_z is barely changed when ν is further increased from 100 to 150. We note that a similar trend can be obtained for the other two principal axes of inertia.

C. Applications to other proteins

To further validate our model, we compare the dependence of $\widetilde{D}_t^{\infty}$ and $\widetilde{D}_r^{\infty}$ on ν for different types of proteins in Fig. 6. Interestingly, the results indicate that the values of $\widetilde{D}_t^{\infty}$ at fixed ν for different types of proteins (i.e., ubiquitin, lysozyme, β-lactoglobulin, and streptavidin) are so close that the $\widetilde{D}_t^{\infty}$–ν relations for different proteins can be mapped onto a master curve of exponential decay, as shown in Fig. 6(a). The same scaling behavior is also observed for the $\widetilde{D}_r^{\infty}$–ν relations, as presented in Fig. 6(b). The translational and rotational diffusion coefficients predicted by the SE relation (based on experimental values of the hydrodynamic radius R_h) are, respectively, obtained at $\widetilde{D}_t^{\infty} = 1$ and $\widetilde{D}_r^{\infty} = 1$, indicated by dashed lines. For both Figs. 6(a) and 6(b), the solid and dashed lines intersect at around $\nu = 25$, which means both translational and rotational diffusion coefficients can meet with the prediction of the SE relation under the same frictional constant. The values of ν_t, ν_r, and $\Delta\nu = |\nu_r - \nu_t|$ for each type of protein are summarized in Table V. Although ν_t and ν_r vary from 12 to 50, for different types of proteins, we always have $\Delta\nu < 10$. The results unveil the scaling behavior behind the model, which follows the prediction of the SE relation.

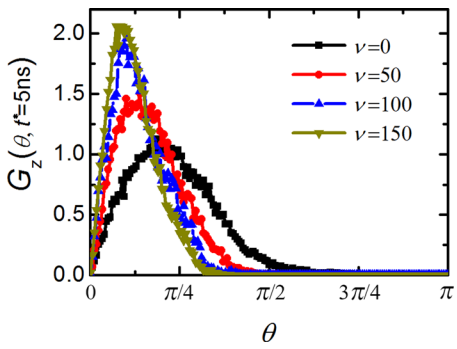

FIG. 5. Angular distribution of the Green function $G_z(\theta)$ corresponding to the third principal axis of inertia z at $t* = 5$ ns for the PSM. The function at each ν is obtained by averaging simulation results with different box sizes.

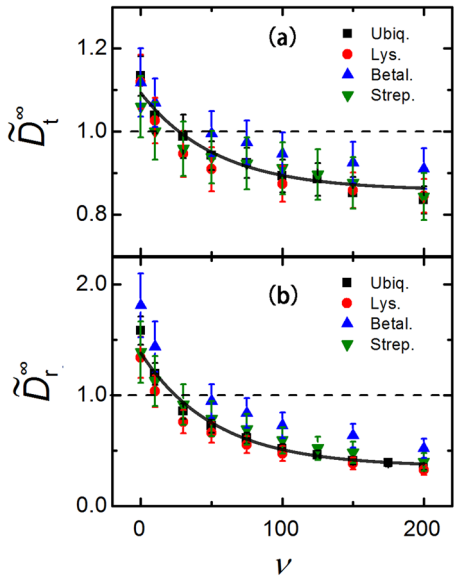

FIG. 6. Dependence of the (a) dimensionless translational diffusion coefficient $\widetilde{D}_t^{\infty}$ and (b) dimensionless rotational diffusion coefficient $\widetilde{D}_r^{\infty}$ in bulk on the fluid–protein frictional constant ν for ubiquitin (black), lysozyme (red), β-lactoglobulin (blue), and streptavidin (olive). All simulations are performed with the PSM. The solid lines are exponential fittings to all data points. The dashed lines are for $\widetilde{D}_t^{\infty} = 1$ and $\widetilde{D}_r^{\infty} = 1$.

TABLE V. Comparisons of ν_t, ν_r, and $\Delta\nu$ for different types of proteins.

Protein type	ν_t	ν_r	$\Delta\nu$
Ubiquitin	29	25	4
Lysozyme	16	12	4
β-Lactoglobulin	48	50	2
Streptavidin	17	26	9

Such universality indicates the model can be applied to simulate the global diffusion for other types of proteins or even other types of macromolecules.

IV. CONCLUSIONS

We, in this work, present a DPD model with the smeared-charge Coulombic potential and tunable-slip interactions for simulating the translational and rotational diffusion of various proteins. The protein could be represented by either mono-sized or poly-sized DPD beads. In comparison, although D_t^{∞} and D_r^{∞} are slightly overestimated, the MSM is fine enough to characterize the diffusion of the protein. While the translational diffusion coefficient D_t increases linearly with the box size, we do not observe the size effect on the rotational diffusion coefficient D_r. The diffusion coefficients in bulk (D_t^{∞} and D_r^{∞}) decrease exponentially with the fluid–protein frictional constant ν. Interestingly, normalized by the diffusion coefficients predicted by the SE relation, both the dimensionless translational diffusion coefficient $\widetilde{D}_t^{\infty}$ and the dimensionless rotational diffusion coefficient $\widetilde{D}_r^{\infty}$ converge for the four different types of proteins. Such scaling behavior indicates correct Navier–Stokes hydrodynamic interactions are included in our model. In addition, the theoretical predictions of both translational and rotational diffusion coefficients based on the SE relation (i.e., $\widetilde{D}_t^{\infty} = 1$ and $\widetilde{D}_r^{\infty} = 1$) are reached simultaneously at around $\nu = 25$.

Aside from the self-diffusion of a single protein, the model has potential applications in simulating unconventional transport and collective behavior without structural changes (internal degrees of freedom). For instance, as the size of the simulation box is much larger than the size of the protein (see Table IV), it is feasible to study the dynamics of multiple proteins. However, simulations of more than one protein molecule will inevitably introduce protein–protein interactions that have not yet been addressed in our current model. A more realistic force[39,67,68] could be introduced as the conservative term of protein–protein interactions, which is parameterized based on techniques such as iterative Boltzmann inversion, inverse Monte Carlo, and conditional reversible work.[38,69] We also note that the hypothesis of a protein without conformational changes shall only be applicable to simulate diffusion in a dilute, energetically mild, and equilibrated system, as it ignores structural changes in some extreme conditions and the role of many-body hydrodynamics in macromolecular crowding (see the supplementary material). Due to the coupled dynamics of the protein and counter-ions, the surface charges of the protein could influence the diffusion coefficients.[70] In the future, we would like to investigate the effect of pH (which determines the charges of protein beads) and ionic strength on the diffusion coefficients. To study the diffusion of proteins in a crowded, extreme, or non-equilibrium system, we would also like to develop models at different levels of coarse-graining.

SUPPLEMENTARY MATERIAL

See the supplementary material for more discussions on parameters for the protein and fluid model, dynamics without frictional forces, D_r determined from time-correlation function, the size effect, and the hydrodynamic radius R_h.

ACKNOWLEDGMENTS

This work was supported by the National Key Research and Development Program of China (Grant No. 2016YFA0501601), NSFC Basic Science Center Program for "Multiscale Problems in Nonlinear Mechanics" (Grant No.11988102), National Natural Science Foundation of China (Grant No. 11602279), and Strategic Priority Research Program of Chinese Academy of Sciences (Grant No. XDB22040102).

DATA AVAILABILITY

The data that support the findings of this study are available from the corresponding author upon reasonable request.

REFERENCES

[1] M. Rabe, D. Verdes, and S. Seeger, Adv. Colloid Interface Sci. **162**, 87 (2011).
[2] I. Firkowska-Boden, X. Zhang, and K. D. Jandt, Adv. Healthcare Mater. **7**, 1700995 (2018).

[3]X. Quan, J. Liu, and J. Zhou, Curr. Opin. Colloid Interface Sci. **41**, 74 (2019).
[4]P. Roach, D. Farrar, and C. C. Perry, J. Am. Chem. Soc. **127**, 8168 (2005).
[5]T. Wei, M. A. Carignano, and I. Szleifer, J. Phys. Chem. B **116**, 10189 (2012).
[6]S. J. Attwood, R. Kershaw, S. Uddin, S. M. Bishop, and M. E. Welland, J. Mater. Chem. B **7**, 2349 (2019).
[7]E. C. Yusko, B. R. Bruhn, O. M. Eggenberger, J. Houghtaling, R. C. Rollings, N. C. Walsh, S. Nandivada, M. Pindrus, A. R. Hall, D. Sept, J. Li, D. S. Kalonia, and M. Mayer, Nat. Nanotechnol. **12**, 360 (2017).
[8]S. Zeng, C. Wen, P. Solomon, S.-L. Zhang, and Z. Zhang, Nat. Nanotechnol. **14**, 1056 (2019).
[9]J. Houghtaling, C. Ying, O. M. Eggenberger, A. Fennouri, S. Nandivada, M. Acharjee, J. Li, A. R. Hall, and M. Mayer, ACS Nano **13**, 5231 (2019).
[10]E. Duboué-Dijon, P. Delcroix, H. Martinez-Seara, J. Hladílková, P. Coufal, T. Křížek, and P. Jungwirth, J. Phys. Chem. B **122**, 5640 (2018).
[11]M. Firnkes, D. Pedone, J. Knezevic, M. Döblinger, and U. Rant, Nano Lett. **10**, 2162 (2010).
[12]M. Boukhet, F. Piguet, H. Ouldali, M. Pastoriza-Gallego, J. Pelta, and A. Oukhaled, Nanoscale **8**, 18352 (2016).
[13]P. R. Cullis, M. J. Hope, M. B. Bally, T. D. Madden, L. D. Mayer, and D. B. Fenske, Biochim. Biophys. Acta **1331**, 187 (1997).
[14]P.-H. Lee, V. Helms, and T. Geyer, J. Chem. Phys. **137**, 145105 (2012).
[15]M. Muthukumar, J. Chem. Phys. **141**, 081104 (2014).
[16]S. K. Kannam and M. T. Downton, J. Chem. Phys. **146**, 054108 (2017).
[17]C. C. Wells, D. V. Melnikov, and M. E. Gracheva, J. Chem. Phys. **147**, 054903 (2017).
[18]I. A. Jou, D. V. Melnikov, and M. E. Gracheva, Nanotechnology **27**, 205201 (2016).
[19]Z. Liu, X. Shi, and H. Wu, Nanotechnology **30**, 165701 (2019).
[20]T. Ding, A. K. Chen, and Z. Lu, Sci. Bull. **64**, 1456 (2019).
[21]N. Haridasan, S. K. Kannam, S. Mogurampelly, and S. P. Sathian, J. Phys. Chem. B **123**, 4825 (2019).
[22]N. Haridasan, S. K. Kannam, S. Mogurampelly, and S. P. Sathian, Phys. Rev. E **97**, 062415 (2018).
[23]G. Kikugawa, T. Nakano, and T. Ohara, J. Chem. Phys. **143**, 024507 (2015).
[24]I.-C. Yeh and G. Hummer, J. Phys. Chem. B **108**, 15873 (2004).
[25]M. Linke, J. Köfinger, and G. Hummer, J. Phys. Chem. B **122**, 5630 (2018).
[26]M. Linke, J. Köfinger, and G. Hummer, J. Phys. Chem. Lett. **9**, 2874 (2018).
[27]P.-c. Chen, M. Hologne, and O. Walker, J. Phys. Chem. B **121**, 1812 (2017).
[28]G. Nawrocki, A. Karaboga, Y. Sugita, and M. Feig, Phys. Chem. Chem. Phys. **21**, 876 (2019).
[29]A. Polimeno and M. Zerbetto, Phys. Chem. Chem. Phys. **21**, 3662 (2019).
[30]V. Wong and D. A. Case, J. Phys. Chem. B **112**, 6013 (2008).
[31]M. Dlugosz and J. M. Antosiewicz, J. Chem. Theory Comput. **10**, 481 (2014).
[32]M. Oura, J. Yamamoto, H. Ishikawa, S. Mikuni, R. Fukushima, and M. Kinjo, Sci. Rep. **6**, 31091 (2016).
[33]M. C. Fink, K. V. Adair, M. G. Guenza, and A. H. Marcus, Biophys. J. **91**, 3482 (2006).
[34]S. Averick, O. Karácsony, J. Mohin, X. Yong, N. M. Moellers, B. F. Woodman, W. Zhu, R. A. Mehl, A. C. Balazs, T. Kowalewski, and K. Matyjaszewski, Angew. Chem., Int. Ed. Engl. **53**, 8050 (2014).
[35]R. Ishima and D. A. Torchia, Nat. Struct. Mol. Biol. **7**, 740 (2000).
[36]J. G. D. La Torre, M. L. Huertas, and B. Carrasco, Biophys. J. **78**, 719 (2000).
[37]A. Stradner and P. Schurtenberger, Soft Matter **16**, 307 (2020).
[38]S. Kmiecik, D. Gront, M. Kolinski, L. Wieteska, A. E. Dawid, and A. Kolinski, Chem. Rev. **116**, 7898 (2016).
[39]S. J. Marrink, H. J. Risselada, S. Yefimov, D. P. Tieleman, and A. H. De Vries, J. Phys. Chem. B **111**, 7812 (2007).
[40]A. Ghavami, E. van der Giessen, and P. R. Onck, J. Chem. Theory Comput. **9**, 432 (2012).
[41]A. Ghavami, L. M. Veenhoff, E. van der Giessen, and P. R. Onck, Biophys. J. **107**, 1393 (2014).
[42]P. Español and P. B. Warren, J. Chem. Phys. **146**, 150901 (2017).
[43]R. D. Groot and P. B. Warren, J. Chem. Phys. **107**, 4423 (1997).
[44]G. Kacar, E. A. J. F. Peters, and G. de With, Europhys. Lett. **102**, 40009 (2013).
[45]A. Maiti and S. McGrother, J. Chem. Phys. **120**, 1594 (2004).
[46]M. Wan, L. Gao, and W. Fang, PLoS One **13**, e0198049 (2018).
[47]E. K. Peter, K. Lykov, and I. V. Pivkin, Phys. Chem. Chem. Phys. **17**, 24452 (2015).
[48]A. Vishnyakov, D. S. Talaga, and A. V. Neimark, J. Phys. Chem. Lett. **3**, 3081 (2012).
[49]A. Baumketner and W. Cai, Phys. Rev. E **98**, 032419 (2018).
[50]C. Li, X. Fu, W. Zhong, and J. Liu, ACS Omega **4**, 10216 (2019).
[51]I. Pagonabarraga, B. Rotenberg, and D. Frenkel, Phys. Chem. Chem. Phys. **12**, 9566 (2010).
[52]K. A. Terrón-Mejía, R. López-Rendón, and A. G. Goicochea, J. Phys.: Condens. Matter **28**, 425101 (2016).
[53]J. Zhou, J. Smiatek, E. S. Asmolov, O. I. Vinogradova, and F. Schmid, "Application of tunable-slip boundary conditions in particle-based simulations," in *High Performance Computing in Science and Engineering '14* (Springer, 2015).
[54]S. Plimpton, J. Comput. Phys. **117**, 1 (1995).
[55]L. E. Thompson and D. Rovnyak, Biochem. Mol. Biol. Educ. **35**, 49 (2007).
[56]D. K. Wilkins, S. B. Grimshaw, V. Receveur, C. M. Dobson, J. A. Jones, and L. J. Smith, Biochemistry **38**, 16424 (1999).
[57]A. Bonincontro, V. Calandrini, and G. Onori, Colloids Surf., B **21**, 311 (2001).
[58]B. Batas, H. R. Jones, and J. B. Chaudhuri, J. Chromatogr. A **766**, 109 (1997).
[59]P. Aymard, D. Durand, and T. Nicolai, Int. J. Biol. Macromol. **19**, 213 (1996).
[60]A. M. M. Van Teeffelen, K. Broersen, and H. H. J. de Jongh, Protein Sci. **14**, 2187 (2005).
[61]B.-Y. Cao and R.-Y. Dong, J. Chem. Phys. **140**, 034703 (2014).
[62]D. Roy, N. Patel, S. Conte, and M. Maroncelli, J. Phys. Chem. B **114**, 8410 (2010).
[63]T. G. Lombardo, P. G. Debenedetti, and F. H. Stillinger, J. Chem. Phys. **125**, 174507 (2006).
[64]L. D. Favro, Phys. Rev. **119**, 53 (1960).
[65]Y. Shim, D. Jeong, M. Y. Choi, and H. J. Kim, J. Chem. Phys. **125**, 061102 (2006).
[66]V. Hornak, R. Abel, A. Okur, B. Strockbine, A. Roitberg, and C. Simmerling, Proteins **65**, 712 (2006).
[67]K. Okuwaki, H. Doi, K. Fukuzawa, and Y. Mochizuki, Appl. Phys. Express **13**, 017002 (2019).
[68]J. K. Brennan, M. Lísal, J. D. Moore, S. Izvekov, I. V. Schweigert, and J. P. Larentzos, J. Phys. Chem. Lett. **5**, 2144 (2014).
[69]G. Deichmann, V. Marcon, and N. F. A. van der Vegt, J. Chem. Phys. **141**, 224109 (2014).
[70]D. R. Grisham and V. Nanda, Proteins: Struct., Funct., Bioinf. **86**, 515 (2018).